Photonic crystal circuits: Localized modes and waveguide couplers

Arthur R. McGurn*
Department of Physics, Western Michigan University, Kalamazoo, Michigan 49008
(Received 24 May 2000; revised manuscript received 22 November 2000; published 16 January 2002)

Localized modes and waveguide couplers in photonic crystal circuits are discussed. Emphasis is placed on circuit geometries which include waveguide channels containing dielectric barriers, channel bends, or junctions with other waveguides. Photonic crystal circuits composed of waveguide channels of both linear and nonlinear dielectric materials are treated. A waveguide coupler which allows energy to be transfered from one waveguide channel to another through weak interchannel interactions is studied.

DOI: 10.1103/PhysRevB.65.1554XX PACS number(s): 42.70.Qs, 42.81.Qb

I. INTRODUCTION

Recently the electromagnetic modes of certain types of photonic crystal circuits have been studied in terms of tight-binding models.[1–3] The tight-binding model formulation characterizes the fields in the circuit channels by sets of differences equations with solutions given as closed formed expressions involving elementary functions. Reference 1 gives a discussion of the propagating mode solutions for a variety of such photonic crystal circuits including those containing dielectric barriers, junctions of waveguide channels, optical switches, and waveguide channels connected by short links. The transmission and reflection of electromagnetic modes entering circuit input leads, reflected by or propagated through the circuit, and exiting through output leads were obtained. The properties of nonlinear photonic crystal circuits were studied in Refs. 2 and 3.

In this paper the theory in Ref. 1 is extended to treat nonpropagating circuit modes. These are a different class of modes which are localized excitations, bound to a subnetwork of the photonic crystal circuit, and not exhibiting transmission and reflection properties. In some instances the localized modes in waveguides formed from nonlinear media are discussed as an extension of the work in Refs. 2 and 3. A study of the modes of waveguide couplers[4] is also presented. The waveguide coupler is formed between two infinitely long waveguides by a weak link interaction between a finite length of the two channels which can transfer energy between the two waveguides. This is the photonic crystal circuit analogy of fiber optics couplers.

In this paper many of the same circuits and sets of difference equations found in Ref. 1 are considered. Consequently, only a brief review of the difference equation formulation and an abbreviated discussion of the circuit geometries and the equations which describe them are given. Schematic drawings are presented of the photonic crystal circuits treated in this paper, but with most of the schematics the reader is referred to Ref. 1 for the associated set of difference equations. To facilitate cross reference, the notation used in Ref. 1 is adopted here.

Following Ref. 1, a two-dimensional photonic crystal formed as a square lattice array of infinitely long, parallel, identical dielectric cylinders[1,5,6] is considered. The periodic dielectric constant of such a system is given by

$$\epsilon(\vec{r}_{||})=\begin{cases}\epsilon, & |\vec{r}_{||}-na_c\hat{i}-ma_c\hat{j}|\leqslant R \text{ for } n \text{ and } m \text{ integers}\\ 1, & \text{otherwise,}\end{cases} \tag{1}$$

where $\vec{r}_{||}=x\hat{i}+y\hat{j}$, a_c is the lattice constant, and $R<a_c/2$ is the radius of the dielectric cylinders. The electromagnetic modes of interest to us are translationally invariant along the z axis with an electric field polarized along the z axis.

A waveguide channel is formed by adding impurity material to a row of cylinders.[1,5,6] The total dielectric constant of the waveguide segment, $\epsilon_T(\vec{r}_{||})$, is given by $\epsilon_T(\vec{r}_{||})=\epsilon(\vec{r}_{||})+\delta\epsilon(\vec{r}_{||})$ where $\delta\epsilon(\vec{r}_{||})$ is the change in the photonic crystal dielectric constant due to impurity material. For a straight waveguide

$$\delta\epsilon(\vec{r}_{||})=\begin{cases}\delta\epsilon, & |x-nra_c|,|y-nsa_c|\leqslant t \text{ for } \{n\} \text{ integers}\\ 0, & \text{otherwise,}\end{cases} \tag{2}$$

where r and s are fixed integers, the length of the waveguide segment depends on the range of the consecutive integers $\{n\}$, $2t\ll R$ is the length of a side of one of the single-site impurities. General circuit geometries are formed by piecing together waveguide segments with a variety of lengths and slopes in the $x-y$ plane.

Using standard techniques,[1,5–7] the electric fields of the photonic crystal waveguide and circuit modes can be written in the form

$$E(\vec{r}_{||}|t)=E^0(\vec{r}_{||},\omega)\exp(-i\omega t), \tag{3}$$

where $E^0(\vec{r}_{||},\omega)$ satisfies

$$E^0(\vec{r}_{||},\omega)=\int d^2r'_{||}G(\vec{r}_{||},\vec{r}'_{||}|\omega)\,\delta\epsilon(\vec{r}'_{||})\left(\frac{\omega}{c}\right)^2 E^0(\vec{r}'_{||},\omega). \tag{4}$$

Here $G(\vec{r}_{||},\vec{r}'_{||}|\omega)$ is the Green's function of the Helmholtz operator, $\nabla^2+\epsilon(\vec{r}_{||})(\omega/c)^2$.

Following Ref. 1, the impurity material in each cylinder is assumed to be of small enough cross-sectional area in the $x-y$ plane so that the electromagnetic field in it is constant. For impurity material centered on the lattice site (nra_c,nsa_c) where n, r, s are integers, the field in the impurity material is denoted by $E_{nr,ns}$ where $E_{nr,ns}=E^0[n(r\hat{i}$

$+s\hat{j})a_c,\omega]$. In a straight segment of waveguide channel with slope s/r, Eq. (4) reduces to the difference equation

$$E_{nr,ns}=\delta\epsilon\sum_m B_{nr,ns;mr,ms}E_{mr,ms}. \tag{5}$$

Here

$$B_{nr,ns;mr,ms}=\left(\frac{\omega}{c}\right)^2\int_{(mr,ms)^{th}impurity}d^2r_{||} \times G[n(r\hat{i}+s\hat{j})a_c,\vec{r}_{||}|\omega], \tag{6}$$

and m runs over the integers denoting the waveguide channel sites.[1] A photonic crystal circuit, composed of a number of such waveguide segments, is described by a set of difference equations of the form of Eq. (5) for each of the waveguide segments composing the circuit. As further simplification, in many instances Eq. (5) can be restricted to same site and nearest-neighbor couplings. (As noted in Refs. 1 and 6, the Green's function at frequencies in the stop gap can decay rapidly in space, particularly near the center of the stop gap. The rate of decay depends on the photonic crystal and the stop gap being considered. For the numerical results from Refs. 1 and 6, used to illustrate the theory in this paper, nearest-neighbor interactions are adequate for a good representation of the properties of the system.) The difference equations with these restrictions are

$$E_{nr,ns}=\gamma[\alpha(0,0)E_{nr,ns}+\alpha(r,s)(E_{(n+1)r,(n+1)s} +E_{(n-1)r,(n-1)s})]. \tag{7}$$

Here $\alpha(0,0)=B_{0,0;0,0}/(4t^2)$, $\alpha(r,s)=B_{0,0;r,s}/(4t^2)$ where r and s are defined in Eqs. (5) and (6), and $\gamma=4t^2\delta\epsilon$. The solutions of Eq. (7) are obtained by choosing ω to be a frequency in the stop band of the photonic crystal, computing $\alpha(0,0)$ and $\alpha(r,s)$, and solving Eq. (7) for $\{E_{nr,ns}\}$ and γ (i.e., $\delta\epsilon$) characterizing the modes.

The simplest example of Eq. (7) is that of a single-site impurity for which

$$E_{0,0}=\gamma_s\alpha(0,0)E_{0,0}. \tag{8}$$

Here γ_s is the value of γ needed to support a single-site impurity, so that $\gamma_s=4t^2\delta\epsilon_s$ gives $\delta\epsilon_s=(1/4t^2)[\alpha(0,0)]^{-1}$. This result will be used for comparison in our discussions below.

The theory of this paper will be illustrated by numerical results generated in Refs. 1 and 6. These are for a square lattice photonic crystal with $\epsilon=9$, $R=0.377\,96a_c$ with frequencies in the $0.425<\omega a_c/2\pi c<0.455$ stop gap for nearest-neighbor waveguide channels with $t=0.01a_c$ or $t=0.1a_c$. In this stop gap the $\alpha(0,0)$ and $\alpha(1,0)$ coefficients of Eq. (7) are from Eqs. (A1) and (A2) of Ref. 1, approximately given by

$$\alpha(0,0)=\alpha_c(0,0)+a_1\left(\frac{\omega a_c}{2\pi c}-\frac{\omega_c a_c}{2\pi c}\right), \tag{9}$$

and

$$\alpha(1,0)=\alpha_c(1,0)+b_1\left(\frac{\omega a_c}{2\pi c}-\frac{\omega_c a_c}{2\pi c}\right). \tag{10}$$

Here ω_c is the mid stop gap frequency, $\alpha_c(0,0)$ is the value of $\alpha(0,0)$ at ω_c, $\alpha_c(1,0)$ is the value of $\alpha(1,0)$ at ω_c, and a_1 and b_1 are frequency-independent constants.

We now turn to a discussion of localized waveguide modes in a variety of different waveguide network geometries. This is followed by a treatment of intrinsic localized modes[2,3] at a junction and a treatment of the modes of waveguide couplers.

II. SINGLE-CHANNEL WAVEGUIDES

In this section single-channel waveguides containing single-site impurities, dielectric barriers, and right-angle bends are considered.

A. Single-site impurities

Consider a straight infinitely long waveguide channel containing a single-site impurity.[5] This is schematically represented in Fig. 1(a). In Fig. 1(a) the large black dot is the cylinder forming the impurity site [located at the lattice site (0,0)] and the dielectric medium forming the cylinders in the upper waveguide channel [located in the lattice at $(0,lr)$ for $l=1,2,3,\ldots$] may be different from the dielectric medium forming the cylinders in the lower waveguide channel [located in the lattice at $(0,lr)$ for $l=-1,-2,-3,\ldots$]. The equations describing the waveguide channel are

$$E_{0,lr}=\gamma_l[\alpha(0,0)E_{0,lr}+\alpha(r,0)(E_{0,(l+1)r}+E_{0,(l-1)r})], \tag{11}$$

where $|l|\geqslant 2$, $\gamma_l=\gamma$ for $l\geqslant 2$, $\gamma_l=\gamma_0$ for $l\leqslant -2$,

$$E_{0,\pm r}=\gamma_\pm[\alpha(0,0)E_{0,\pm r}+\alpha(0,r)E_{0,\pm 2r}]+\gamma_1\alpha(0,r)E_{0,0}, \tag{12}$$

where $\gamma_+=\gamma$, $\gamma_-=\gamma_0$, and

$$E_{0,0}=\gamma_1\alpha(0,0)E_{0,0}+\gamma\alpha(0,r)E_{0,r}+\gamma_0\alpha(0,r)E_{0,-r}. \tag{13}$$

Here the impurity located at (0,0) is characterized by the parameters γ_1, $\delta\epsilon_1$; the cylinders forming the upper waveguide channel are characterized by the parameters γ, $\delta\epsilon$; and the cylinders forming the lower waveguide channel are characterized by the parameters γ_0, $\delta\epsilon_0$. The γ, γ_0, and γ_1 can all be different.

A bound-state solution of Eqs. (11)–(13) of the form $E_{0,lr}=ae^{-lq}$ for $l\geqslant 1$, $E_{0,0}=c$, and $E_{0,lr}=be^{lk}$ for $l\leqslant -1$ can be found. This is a mode which has a maximum field intensity at the (0,0) lattice site and a field intensity which goes to zero at an infinite separation from (0,0) for all directions in the $x-y$ plane. Substitution into Eqs. (11)–(13) gives $a=\gamma_1 c/\gamma=\delta\epsilon_1 c/\delta\epsilon$, $b=\gamma_1 c/\gamma_0=\delta\epsilon_1 c/\delta\epsilon_0$, where

$$\gamma=[\alpha(0,0)+2\alpha(0,r)\cosh q]^{-1}, \tag{14}$$

$$\gamma_0=[\alpha(0,0)+2\alpha(0,r)\cosh k]^{-1}. \tag{15}$$

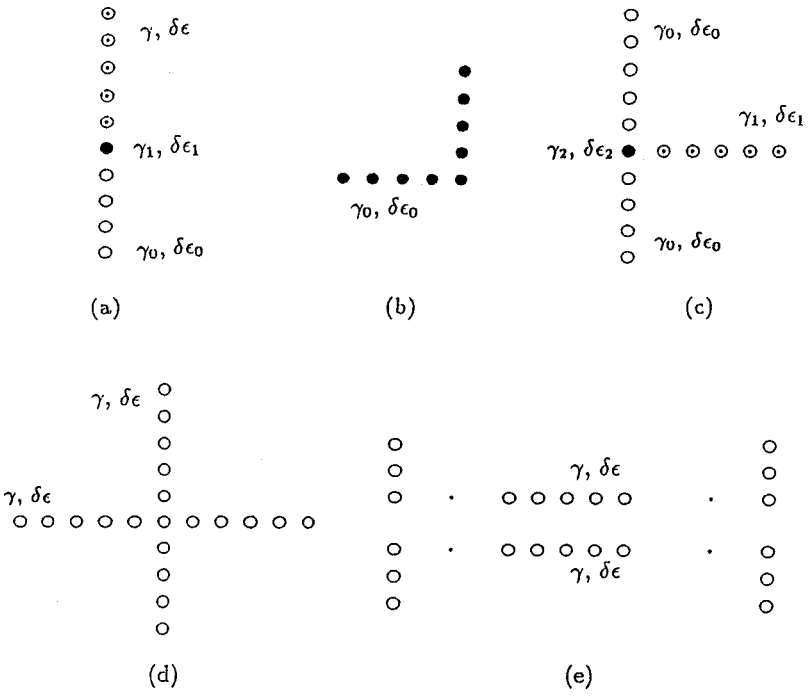

FIG. 1. Schematic plot of waveguide channels for waveguides in a square lattice photonic crystal. Note that only the cylinders of the waveguide channel are shown and the remaining cylinders of the square lattice photonic crystal are not shown. The waveguide channels are labeled with the appropriate γ's and $\delta\epsilon$'s describing the channel dielectric parameters. The x axis in horizontal and the y axis is vertical. The waveguides shown are: (a) waveguide channel with impurity, (b) waveguide with a right-angle bend, (c) junction of an infinite and a semi-infinite waveguide, (d) junction of two infinite waveguides, and (e) waveguide coupler. The different colored circles in these drawings represent different types of impurity materials.

These equations relate q, k, and the couplings in the difference equations to a, b, c, γ, and γ_0. The value of γ_1 required for a bound state at the single-site impurity is given by

$$\gamma_1=[\alpha(0,0)+\alpha(0,r)(e^{-q}+e^{-k})]^{-1}. \tag{16}$$

Once the impurity mode frequency ω is fixed in the stop gap of the photonic crystal and $\alpha(0,0)$ and $\alpha(0,r)$ are computed, Eq. (16) determines the γ_1 needed (or since $\gamma_1=4t^2\delta\epsilon_1$, the $\delta\epsilon_1$ needed) for a bound-state mode with a given set of k and q at frequency ω. The field intensities (a and b) of the mode are set by the parameter c, i.e., the field intensity at the impurity site.

In the limit that k and q become infinite, Eqs. (14)–(16) reduce to the single-site impurity limit, i.e., $\gamma=\gamma_0=0$ and $\gamma_1=\alpha(0,0)^{-1}$. If only k is taken to be infinite, the case of a semi-infinite waveguide which terminates in an impurity is obtained. The medium in the semi-infinite waveguide channel is given by $\gamma=[\alpha(0,0)+2\alpha(0,r)\cosh q]^{-1}$ and the medium at the termination site is $\gamma_1=[\alpha(0,0)+\alpha(0,r)e^{-q}]^{-1}$. If the termination site is of the same medium as that of the waveguide channel, a semi-infinite waveguide will not support a localized mode bound to the termination. For there to be a very weakly localized mode (i.e., in the limit of small k and q), to terms of order k and q, $\gamma=\gamma_0=[\alpha(0,0)+\alpha(0,r)]^{-1}$ and $\gamma_1=[\alpha(0,0)+2\alpha(0,r)(1-q-k)]^{-1}$.

By adjusting the media forming the waveguide channel, the envelop of the bound state can be spread out preferentially in the waveguide channel along one or both channel directions from the impurity site. This may be of application in the design of lasers and other devices in which modes with anisotropic field distributions can be of interest. (These design characteristics are a property of many of the solutions presented in this paper and will be addressed in the Conclusions section.)

As an illustration of the theory, consider the square lattice $\epsilon=9$, $R=0.377\,96a_c$ photonic crystal containing $t=0.01a_c$, $r=1$ or $t=0.1a_c$, $r=1$ waveguide channels.[1,5,6] Writing the γ's in terms of the $\delta\epsilon$'s and using the the numerical data of Refs. 1, 5, and 6 at the mid-gap frequency, $\omega a_c/2\pi c=0.440$ in Eqs. (14)–(16) yields

$$\frac{\delta\epsilon_0}{\delta\epsilon_s}=[1+\rho_1\cosh k]^{-1}, \tag{17}$$

$$\frac{\delta\epsilon}{\delta\epsilon_s}=[1+\rho_1\cosh q]^{-1}, \tag{18}$$

and

$$\frac{\delta\epsilon_1}{\delta\epsilon_s}=[1+\rho_2(e^{-q}+e^{-k})]^{-1}, \tag{19}$$

Here $\rho_1=0.170$, $\rho_2=0.085$ for waveguide channels with $t=0.01a_c$, and $\rho_1=0.374$, $\rho_2=0.187$ for waveguide channels with $t=0.1a_c$. As a comparison with the case of a single-site impurity in an otherwise perfect photonic crystal, we have written Eqs. (17)–(19) in terms of $\delta\epsilon_s$ defined below Eq. (8) and have used the definition of γ_0, γ, and γ_1 in terms of $\delta\epsilon_0$, $\delta\epsilon$, and $\delta\epsilon_1$. Equations (17)–(19) give the conditions needed to observe a bound state at $\omega a_c/2\pi c=0.440$. In Fig. 2 $g_0=\delta\epsilon_0/\delta\epsilon_s$, $g=\delta\epsilon/\delta\epsilon_s$, and $g_1=\delta\epsilon_1/\delta\epsilon_s$ versus k are plotted for fixed $q=3$. Results are shown for both the $t=0.01a_c$ and the $t=0.1a_c$ waveguide channels. The lines labeled (a) present results for $\delta\epsilon_0/\delta\epsilon_s$, the flat lines labeled (b) presents results for $\delta\epsilon/\delta\epsilon_s$, and dotted labeled (c) presents results for $\delta\epsilon_1/\delta\epsilon_s$. In all three sets of lines the results for the systems formed from $t=0.1a_c$ waveguide channels lie below those for the systems formed from $t=0.01a_c$ waveguide channels. In both the t

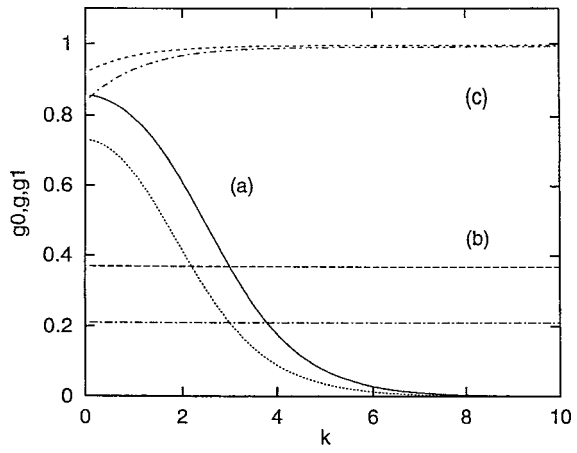

FIG. 2. Plot along the vertical axis of $g_0=\delta\epsilon_0/\delta\epsilon_s$, $g=\delta\epsilon/\delta\epsilon_s$, and $g_1=\delta\epsilon_1/\delta\epsilon_s$ versus k for the system described in Eqs. (11)–(13). In these plots $q=3$ and for the sets of curves labeled (a), (b), (c), the upper curves of the set are for $t=0.01a_c$ waveguide channels, and the lower curves of the set are for $t=0.1a_c$ waveguide channels.

$=0.1a_c$ and the $t=0.01a_c$ systems $q=3$ so that the impurity mode decays quickly away from the γ_1 site in the γ channel. Consequently, as k becomes large so that the impurity mode decays quickly away from the γ_1 site in the γ_0 channel, the value of γ_1 (or $\delta\epsilon_1$) approaches γ_s (or $\delta\epsilon_s$) for a single site in an otherwise pure photonic crystal. In general, all of $\delta\epsilon$, $\delta\epsilon_0$, and $\delta\epsilon_1$ are less than $\delta\epsilon_s$.

To illustrate the frequency dependence in Eqs. (14)–(16), in Fig. 3 additional results are shown for the square lattice photonic crystal and waveguide geometry treated in Fig. 2. In Fig. 3 plots of e^q and $g=\delta\epsilon(\omega)/\delta\epsilon_s(\omega)$ versus frequency are presented for the case in which $q=k$. Both $t=0.01a_c$ and $t=0.1a_c$ types of waveguide channels are considered. For these plots γ_1 has been taken to be equal to the value of γ_s at $\omega a_c/2\pi c=0.440$. In this case, as expected, e^q diverges and γ goes to zero as $\omega a_c/2\pi c$ approaches 0.440. This is the k, q infinite (i.e., $\gamma=\gamma_0=0$) limit discussed above. As the frequency is lowered below 0.440, the impurity wave function in the waveguide channel is seen to contract around the impurity site and the dielectric strength of the waveguide channel increases.

To obtain a solution for a single-site impurity made from a Kerr nonlinear medium, γ_1 in Eqs. (11)–(13) is replaced by $\gamma_1(1+\delta|E_{0,0}|^2)$. The solution of the resulting equations is obtained from that of the linear case by replacing γ_1 by $\gamma_1(1+\delta|c|^2)$.

B. Barriers

Consider an infinitely long straight waveguide containing a dielectric barrier. The waveguide channel is located on the lattice sites (lra_c, lsa_c) where r and s are fixed integers defining the slope of the waveguide in the $x-y$ plane and l ranges over the integers. The barrier material is located on the sites labeled $l=-n,-(n-1),\ldots,(n-1),n$ and is characterized by $\gamma_1=4t^2\delta\epsilon_1$ for the material added to the cylinders in the barrier. The remaining sites of the waveguide

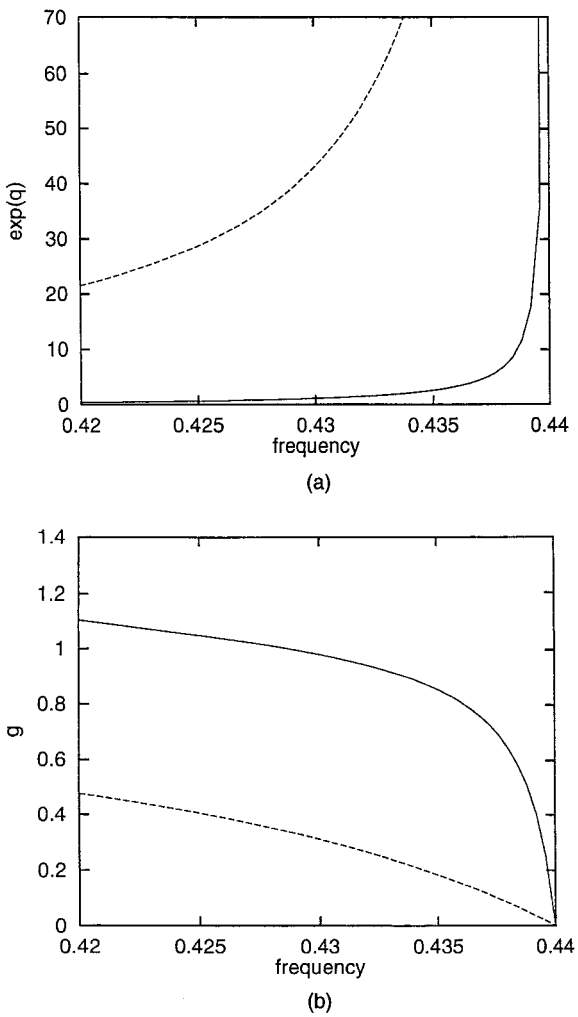

FIG. 3. Plot of: (a) e^q versus frequency $\omega a_c/2\pi c$ for the $t=0.1a_c$ (upper curve) and the $t=0.01a_c$ (lower curve) waveguides, and b) $g=\delta\epsilon/\delta\epsilon_s$ versus frequency $\omega a_c/2\pi c$ for the $t=0.1a_c$ (lower curve) and the $t=0.01a_c$ (upper curve) waveguides. In these plots we consider a system with $q=k$ and a fixed coupling $\gamma_1=4t^2\delta\epsilon_1$ as described in the text.

are characterized by $\gamma_0=4t^2\delta\epsilon_0$ for the material forming the channel outside the barrier. The set of difference equations for this system can be found in Eqs. (25)–(28) of Ref. 1.

A set of localized electromagnetic modes are bound to the barrier material. The fields of these modes in the impurity materials forming the waveguide channel and the barrier are of the form

$$E_{lr,ls}=a_l e^{-q|l|}, \tag{20}$$

where $l=\pm(n+1),\pm(n+2),\ldots,$ with $a_l=a$ for $l\geqslant(n+1)$, $a_l=b$ for $l\leqslant-(n+1)$, and

$$E_{lr,ls}=ce^{ikl}+de^{-ikl}, \tag{21}$$

where $l=0,\pm1,\pm2,\ldots,\pm n$. The coefficients a, b, c, d, and the values of γ_0 and γ_1 for modes of frequency ω in the stop gap are determined from the set of waveguide difference equations [see Eqs. (25)–(28) of Ref. 1]. Substituting Eqs. (20) and (21) into these difference equations gives

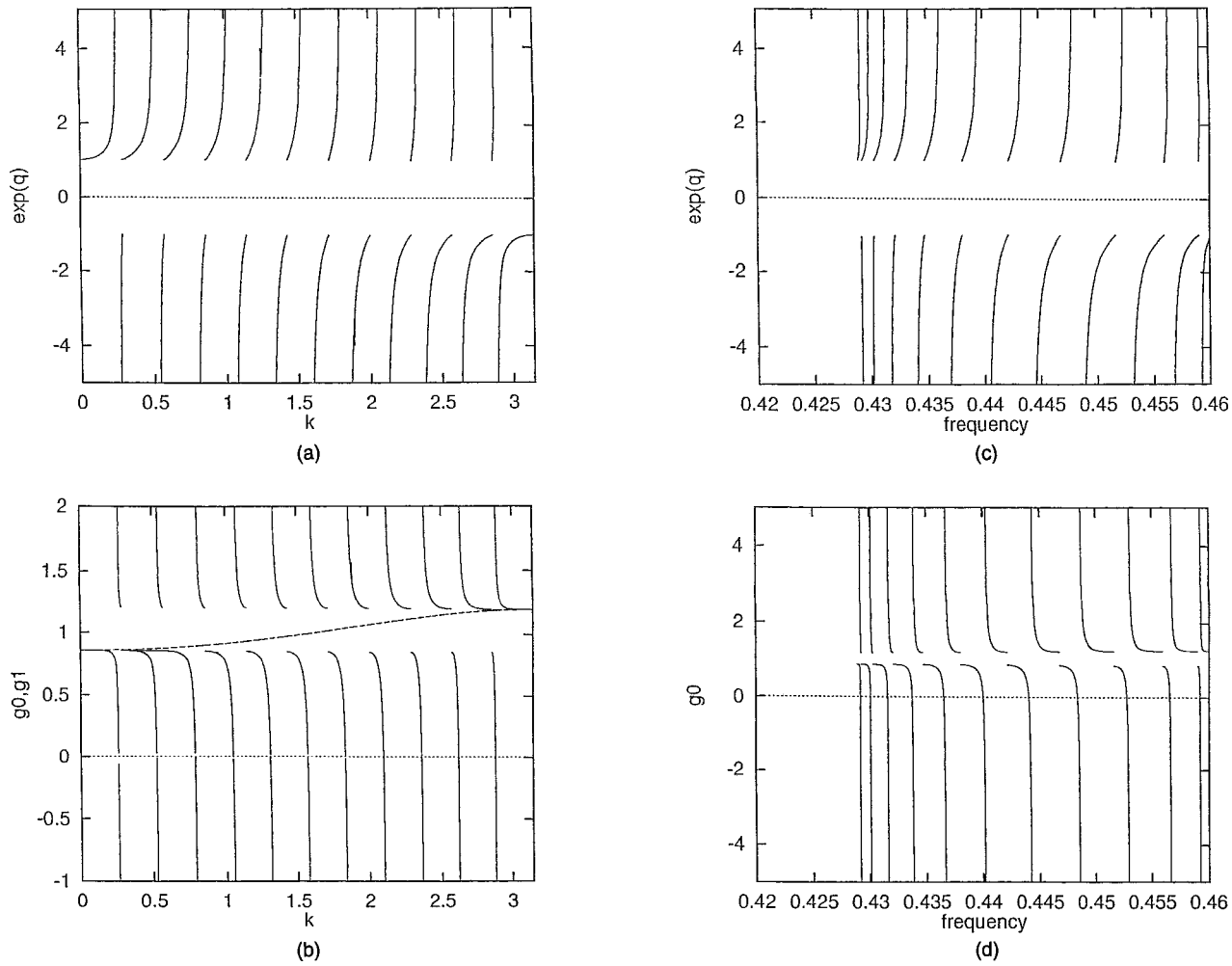

FIG. 4. (a) Plot of e^q versus k solution of Eq. (25). (b) Plot along the vertical axis of $g_0=\delta\epsilon_0/\delta\epsilon_s$ (solid curve) and $g_1=\delta\epsilon_1/\delta\epsilon_s$ (dashed curve) versus k for the system in Eq. (24). (c) Plot of e^q versus frequency $\omega a_c/2\pi c$ for the case of fixed γ_1 described in the text. (d) Plot of g_0 versus frequency $\omega a_c/2\pi c$ for the case of fixed γ_1 described in the text.

$$\gamma_0=[\alpha(0,0)+2\alpha(r,s)\cosh q]^{-1}, \tag{22}$$

$$\gamma_1=[\alpha(0,0)+2\alpha(r,s)\cos k]^{-1}, \tag{23}$$

and the matrix equation

$$\begin{vmatrix} b_{11} & b_{12} & b_{13} & b_{14} \\ b_{21} & b_{22} & b_{23} & b_{24} \\ b_{31} & b_{32} & b_{33} & b_{34} \\ b_{41} & b_{42} & b_{43} & b_{44} \end{vmatrix} \begin{vmatrix} a \\ b \\ c \\ d \end{vmatrix} = 0, \tag{24}$$

where $b_{11}=b_{22}=\gamma_0 e^{-q(n+1)}$, $b_{31}=b_{42}=\gamma_0 e^{-qn}$, $b_{12}=b_{21}=b_{32}=b_{41}=0$, $b_{13}=b_{24}=b_{14}^*=b_{23}^*=-\gamma_1 e^{ik(n+1)}$, and $b_{33}=b_{44}=b_{34}^*=b_{43}^*=-\gamma_1 e^{ikn}$. The condition for Eq. (24) to have a solution is that

$$e^{-2q}\sin 2kn-2e^{-q}\sin(2n+1)k+\sin 2k(n+1)=0. \tag{25}$$

From Eq. (25) we find that Eqs. (20) and (21) yield a solution provided that $e^{-q}=\sin(2n+1)k/\sin 2nk\pm\{[\sin(2n+1)k/\sin 2nk]^2-\sin 2(n+1)k/\sin 2nk\}^{1/2}$ and $-1\leqslant e^{-q}\leqslant 1$. Once k and q have been set, Eqs. (22) and (23) give the impurity strengths of the waveguide channel and barrier materials needed to support the mode.

In the limit that q becomes infinite $\gamma_0=0$, and Eqs. (22), (23), and (25) correctly give the conditions for localized modes to exist on a finite waveguide segment of length $2n+1$. In this limit the discrete set of modes in the finite segment are of the form of Eq. (21) for k a solution of $\sin 2(n+1)k=0$. In the other extreme of very weakly bound modes, e^q approaches ± 1 and k are determined from $\sin 2kn-\pm\sin(2n+1)k+\sin k(n-1)=0$.

As an illustration of the theory, consider the $\epsilon=9$, $R=0.377\,96a_c$ photonic crystal with $t=0.01a_c$ and $(r,s)=(1,0)$ waveguide channels for an impurity mode of frequency $\omega a_c/2\pi c=0.440$ in the mid gap. From Eq. (25) the values of e^q versus k for bound states are found. A plot of these is given in Fig. 4(a) for $n=5$. A discrete sent of intervals in (k,q) space is found. Outside of these intervals no localized modes are found. Next consider the values of γ_0 and γ_1 required to observe localized barrier modes of a particular k, q. Figure 4(b) presents results for $g_0=\delta\epsilon_0/\delta\epsilon_s$ and

$g_1=\delta\epsilon_1/\delta\epsilon_s$ versus k from Eqs. (22) and (23) for $\omega a_c/2\pi c=0.440$. (Again we have written the γ's in terms of $\delta\epsilon$'s.) Here $\delta\epsilon_s$ is the value of $\delta\epsilon$ [obtained below Eq. (8)] for a single site defect of frequency $\omega a_c/2\pi c=0.440$. In Fig. 4(b) the solid line shows results for $g_0=\delta\epsilon_0/\delta\epsilon_s$, while the dashed line shows results for $g_1=\delta\epsilon_1/\delta\epsilon_s$. The results for $\delta\epsilon_0/\delta\epsilon_s$ exhibit a stronger dependence on k than do those for $\delta\epsilon_1/\delta\epsilon_s$ due to the $\cosh q$ factor in Eq. (22) and the strong dependence of q on k. An interesting feature in the physics of the barrier problem, from that of the single-site impurity discussed in Sec. II A, is that e^q can be both positive or negative.

In Figs. 4(c) and (d) plots demonstrating the frequency dependence of the barrier results are shown for e^q and $g_0=\delta\epsilon_0(\omega)/\delta\epsilon_s(\omega)$ versus frequency ω. Here γ_1 has been taken to be equal to γ_s evaluated at $\omega a_c/2\pi c=0.440$, and a number of solutions are found for both positive and negative values of e^q.

C. Bend

Consider a waveguide with a right-angle bend in its channel.[1] [In Fig. 1(b) we present a schematic figure of the waveguide channel indicating the γ_0 and $\delta\epsilon_0$ characterizing the cylinders forming the waveguide channel.] The waveguide is in a square lattice photonic crystal. One part of the waveguide channel is on the negative x axis and the other part is on the positive y axis. As in the considerations in Ref. 1 of this geometry, for propagating mode solutions, both nearest- and next-nearest-neighbor couplings in the waveguide equations are included. Next-nearest-neighbor couplings are included as they distinguish between straight waveguides and waveguides with right-angle channel bends. The waveguide channel is taken to be of a single type of dielectric impurity material. The difference equations for this system are obtained from Eq. (4), and the reader is referred to Eqs. (42)–(46) of Ref. 1 for a detailed presentation of these equations along with a discussion of their propagating mode solutions.

Solutions for modes bound at the right-angle bend are of the form

$$E_{lr,0}=ae^{ql}, \tag{26}$$

where $l=-1,-2,\ldots,$

$$E_{0,lr}=be^{-ql}, \tag{27}$$

where $l=1,2,\ldots,$ and

$$E_{0,0}=h. \tag{28}$$

Substitution of this form into the difference equations gives $\gamma_0=[\alpha(0,0)+\alpha(r,0)\cosh q]^{-1}$ and a matrix equation relation for a, b, h,

$$\begin{vmatrix} a_{11} & a_{12} & a_{13} \\ a_{21} & a_{22} & a_{23} \\ a_{31} & a_{32} & a_{33} \end{vmatrix} \begin{vmatrix} a \\ b \\ h \end{vmatrix} = 0, \tag{29}$$

where $a_{11}=a_{12}=e^{-q}$, $a_{21}=-a_{23}=a_{32}=-a_{33}=-e^q$, $a_{22}=a_{31}=\alpha(r,r)/\alpha(0,r)$, and $a_{13}=-2\cosh q$. For a solution of Eq. (29) to exist,

$$e^{4q}-\left[\left(\frac{\alpha(r,r)}{\alpha(0,r)}\right)^2+1\right]e^{2q}-2\left(\frac{\alpha(r,r)}{\alpha(0,r)}\right)e^q-\left(\frac{\alpha(r,r)}{\alpha(0,r)}\right)^2=0. \tag{30}$$

This gives the q needed for a bound state at frequency ω. In the limit that $|\alpha(r,r)/\alpha(0,r)|\ll 1$, $e^{-q}\approx 1-\alpha(r,r)/\alpha(0,r)$ for $\alpha(r,r)/\alpha(0,r)>0$ or $-[1+\alpha(r,r)/\alpha(0,r)]$ for $\alpha(r,r)/\alpha(0,r)<0$ so that one of these forms will give a mode localized at the channel bend. Whichever of these forms represents the localized mode solution in this limit, the rate of decay of the field of the localized mode away from the bend is governed by $q\approx|\alpha(r,r)/\alpha(0,0)|$. As expected when $\alpha(r,r)$ vanishes the localized mode disappears.

III. WAVEGUIDE JUNCTIONS AND INTRINSIC LOCALIZED MODES

A branched waveguide or waveguide junction is made by attaching a semi-infinite waveguide at a site of an infinite waveguide.[1] [In Fig. (1c) a schematic figure of the junction is shown labeled by the γ's and $\delta\epsilon$'s characterizing the sites of the channel.] For generality it is assumed that the channels of the two waveguides are of different types of impurity materials and the point of attachment is made of a third type of impurity material.

A. Linear media

The difference equations describing the branched waveguide in Fig. 1(c) can be generated from Eq. (5), or the reader can find them in Eqs. (55)–(59) of Ref. 1. The bound-state solutions, localized at the waveguide junction, are of the form

$$E_{0,lr}=b_le^{-q|l|} \tag{31}$$

for $l=\pm 1,\pm 2,\pm 3,\ldots,$ with $b_l=b$ for $b\geqslant 1$, $b_l=c$ for $b_l\leqslant -1$,

$$E_{lr,0}=ae^{-kl} \tag{32}$$

for $l=1,2,3,\ldots,$ and

$$E_{0,0}=d. \tag{33}$$

Substituting these into the difference equations gives

$$\gamma_0=[\alpha(0,0)+2\alpha(r,0)\cosh q]^{-1}, \tag{34}$$

where γ_0 describes the channel material in the infinite waveguide channel, and

$$\gamma_1=[\alpha(0,0)+2\alpha(r,0)\cosh k]^{-1}, \tag{35}$$

where γ_1 describes the channel material in the semi-infinite waveguide channel. Equations (34) and (35) relate the impurity dielectric constants in the two waveguide channels to the mode frequency ω, and k and q. The material at the junction site is described by the parameter γ_2. From the set of difference equations, the coefficients b, c, a, d are related by

$$\begin{vmatrix} \gamma_1\alpha(r,0)e^{-k} & \gamma_0\alpha(r,0)e^{-q} & \gamma_0\alpha(r,0)e^{-q} & -[1-\gamma_2\alpha(0,0)] \\ \gamma_1 & 0 & 0 & -\gamma_2 \\ 0 & \gamma_0 & 0 & -\gamma_2 \\ 0 & 0 & \gamma_0 & -\gamma_2 \end{vmatrix} \begin{vmatrix} a \\ b \\ c \\ d \end{vmatrix} = 0. \tag{36}$$

For a solution of Eq. (36) to exist

$$\gamma_2 = \frac{1}{\alpha(0,0)+\alpha(0,r)(2e^{-q}+e^{-k})}. \tag{37}$$

This gives γ_2 needed for a mode of frequency ω with set values of k and q. In the limit that $q=k$ and $\gamma_0=\gamma_1=\gamma_2=\gamma$, we find that $e^q=\pm\sqrt{2}$ so that $\gamma=2/[2\alpha(0,0)\pm 3\sqrt{2}\alpha(r,0)]$. This case indicates that there will be bound-state modes at the junction of two waveguides with channels formed from the same type of material.

A generalization to the case of two infinitely long straight intersecting waveguides can be made. Consider a waveguide along the x axis intersecting at the origin with a waveguide along the y axis [see Fig. 1(d)]. The equations describing this are

$$E_{lr,0} = \gamma[\alpha(0,0)E_{lr,0} + \alpha(r,0)(E_{(l+1)r,0}+E_{(l-1)r,0})], \tag{38}$$

where $l=\pm 1,\pm 2,\pm 3,\ldots,$

$$E_{0,lr} = \gamma[\alpha(0,0)E_{0,lr} + \alpha(r,0)(E_{0,(l+1)r}+E_{0,(l-1)r})], \tag{39}$$

where $l=\pm 1,\pm 2,\pm 3,\ldots,$

$$E_{0,0} = \gamma[\alpha(0,0)E_{0,0} + \alpha(r,0)(E_{r,0}+E_{-r,0}+E_{0,r}+E_{0,-r})]. \tag{40}$$

Equations (38)–(40) have a solution of the form $E_{lr,0}=E_{0,lr}=de^{-q|l|}$. Substituting gives $\gamma=[\alpha(0,0)+2\alpha(r,0)\cosh q]^{-1}$ for γ in terms of ω and q. The condition that a bound state exists at frequency ω in the stop band is, for $\alpha(0,0)$, and $\alpha(r,0)$ evaluated at ω, $e^q=\pm\sqrt{3}$. This requires that $\gamma=\sqrt{3}/[\sqrt{3}\alpha(0,0)\pm 4\alpha(r,0)]$.

The numerical data in Refs. 1,5 and 6 can be used to illustrate the $\epsilon=9$, $R=0.377\,96a_c$ square lattice photonic crystal with either $t=0.01a_c$, $r=1$ or $t=0.1a_c$, $r=1$ waveguide channels. For the $\gamma_0=\gamma_1=\gamma_2=\gamma=4t^2\delta\epsilon$ limit of the junction in Fig. 1(c), the bound-state condition is $\gamma=4t^2\delta\epsilon=1/[\alpha(0,0)\pm 3\alpha(1,0)/\sqrt{2}]$. For the junction in Eqs. (38)–(40) with $r=1$, the bound state condition is $\gamma=4t^2\delta\epsilon=1/[\alpha(0,0)\pm 4\alpha(1,0)/\sqrt{3}]$. In Fig. 5 plots of $g=\delta\epsilon(\omega)/\delta\epsilon_s(\omega)$ versus $\omega a_c/2\pi c$ in the $0.425\leqslant\omega a_c/2\pi c\leqslant 0.455$ stop gap are presented for these two types of junctions geometries. In these plots results are presented for junctions made either entirely from $t=0.01a_c$ waveguide channels or entirely from $t=0.1a_c$ waveguide channels. The results give an idea of the relative dielectric strengths needed to bind modes at the junction channels compared to the dielectric strength needed to bind an impurity at a isolated single site in the bulk photonic crystal.

B. Kerr nonlinear media

The analysis of junctions can be extended to consider the case of waveguide channels composed of Kerr nonlinear me-

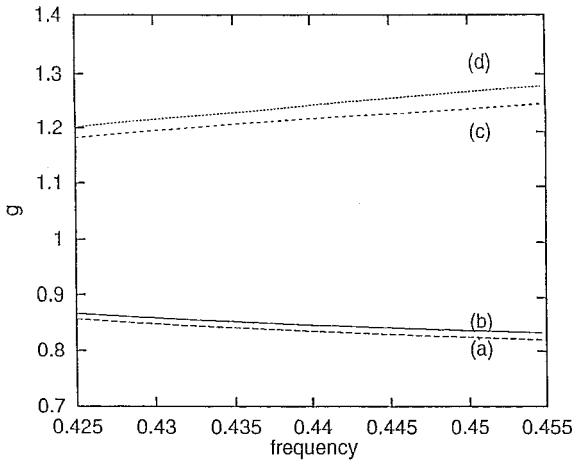

(a)

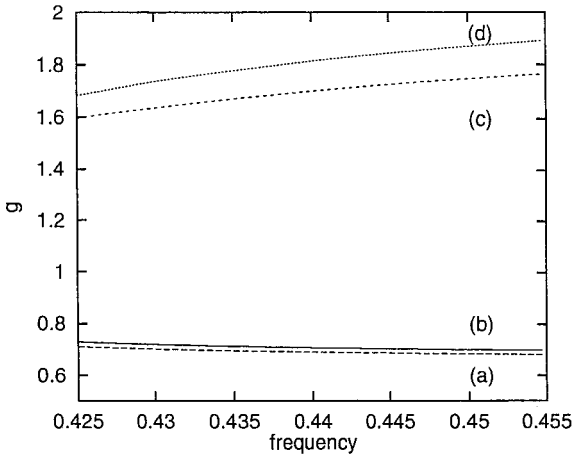

(b)

FIG. 5. Plots of the ratio $g=\delta\epsilon/\delta\epsilon_s$ versus $\omega a_c/2\pi c$ for the junction of an infinite and a semi-infinite waveguide and for the junction of two infinite waveguides. Figure 5(a) is for junctions formed from a system of $t=0.01a_c$ waveguide channels and Fig. 5(b) is for junctions formed from a system of $t=0.1a_c$ waveguides. The lines in these plots are labled as: a) the + root case of the system described in Fig. 1(d), (b) the + root case of the system described in Fig. 1(c), (c) the − root case of the system described in Fig. 1(c), and (d) the − root case of the system described in Fig. 1(d).

dia. Outside of the channels the photonic crystal is formed of linear dielectric materials. In previous publications[2,3,8] it has been shown that a single-channel waveguide formed from Kerr nonlinear media supports both propagating and stationary intrinsic localized modes. The analysis is based on methods developed in the study of intrinsic localized modes in nonlinear vibrational systems[9] and can be extended to show that stationary intrinsic localized modes centered about the junction of an infinite and semi-infinite waveguide with channels of Kerr nonlinear media exist. A junction with the geometry in Fig. 1(c) is considered for the case in which all of the sites of the waveguide channels are composed of an identical Kerr medium.

Following Ref. 2, the junction equations in Eqs. (55)–(59) of Ref. 1, generalized to Kerr nonlinear media, become

$$E_{lr,0}=\gamma[\alpha(0,0)E_{lr,0}+\alpha(0,0)DE_{lr,0}^3+\alpha(r,0)(E_{(l-1)r,0}+E_{(l+1)r,0})+\alpha(r,0)D(E_{(l-1)r,0}^3+E_{(l+1)r,0}^3)], \tag{41}$$

where $l=1,2,3,\ldots,$

$$E_{0,lr}=\gamma[\alpha(0,0)E_{0,lr}+\alpha(0,0)DE_{0,lr}^3+\alpha(r,0)(E_{0,(l-1)r}+E_{0,(l+1)r})+\alpha(r,0)D(E_{0,(l-1)r}^3+E_{0,(l+1)r}^3)], \tag{42}$$

where $l=\pm 1,\pm 2,\pm 3,\ldots,$

$$E_{0,0}=\gamma[\alpha(0,0)E_{0,0}+\alpha(0,0)DE_{0,0}^3+\alpha(r,0)(E_{0,r}+E_{0,-r}+E_{r,0})+\alpha(r,0)D(E_{0,r}^3+E_{0,-r}^3+E_{r,0}^3)]. \tag{43}$$

These equations are obtained from Eq. (4) by taking $\delta\epsilon[(lr\hat{i}+0\hat{j})a_c]=\delta\epsilon[1+D|E_{lr,0}|^2)$ and $\delta\epsilon[(0\hat{i}+lr\hat{j})a_c]=\delta\epsilon(1+D|E_{0,lr}|^2)$.

As in Ref. 2, solutions are sought for highly localized modes of the form

$$E_{0,0}=\alpha, \tag{44}$$

$$E_{0,lr}=E_{lr,0}=\alpha A_0(-1)^l e^{-lq}, \tag{45}$$

where $l=1,2,3,\ldots,$ and $E_{-lr,0}=E_{lr,0}$. (For a good general discussion of the form of this solution and its application to nonlinear difference equations, the reader is also referred to the review by Seivers and Page.[9]) Substituting Eqs. (44) and (45) in Eqs. (41)–(43) gives three nonlinear equations for the parameters characterizing intrinsic localized modes,

$$1/\gamma_0=1+a-3b\Delta-3c\Delta^3, \tag{46}$$

$$1/\gamma_0=\frac{1}{\Delta}[\Delta+a\Delta^3-b(1+\Delta K)-c(1+\Delta^3K^3)], \tag{47}$$

and

$$1/\gamma_0=1-2b\cosh q. \tag{48}$$

Here $\gamma_0=\alpha(0,0)\gamma$, $\Delta=A_0e^{-q}$, and $K=e^{-q}$ are solved for in terms of $a=D\alpha^2$, $b=\alpha(r,0)/\alpha(0,0)$, and $c=ab$ characterizing the couplings and Kerr nonlinearity in the system. From this solution, Δ, K, γ_0 or equivalently γ, A_0, q are given in terms of the mode frequency ω and the coefficient D of the Kerr term.

For highly localized modes (i.e., $|\Delta|$, $|K|\ll 1$), the terms ΔK, Δ^3, and Δ^3K^3 in Eqs. (46) and (47) and the K term in Eq. (48) can be ignored. The solution of the resulting equations is

$$K=\frac{a\pm a[1+12(a+1)b^2/a^2]^{1/2}}{6(a+1)b}, \tag{49}$$

$$\Delta=(a+1)K, \tag{50}$$

$$\gamma_0=\left[1-\frac{b}{K}\right]^{-1}. \tag{51}$$

Using the numerical results in Ref. 1 for the $\omega a_c/2\pi c=0.440$ mode of the $\epsilon=9$, $R=0.377\,96a_c$ square lattice photonic crystal with $t=0.01a_c$ waveguide channels, the minus sign case of Eq. (49) gives

$$K=\frac{D\alpha^2-D\alpha^2[1+0.090(1+D\alpha^2)/(D^2\alpha^4)]^{1/2}}{0.52(1+D\alpha^2)}\approx-\frac{0.087}{D\alpha^2}, \tag{52}$$

$$\Delta=(1+D\alpha^2)K\approx-0.087\left(1+\frac{1}{D\alpha^2}\right), \tag{53}$$

$$\gamma_0=\left[1-\frac{0.087}{K}\right]^{-1}\approx[1+D\alpha^2]^{-1}. \tag{54}$$

These results characterize the shape of the intrinsic localized mode and the value of γ_0 needed for its existence in terms of the coefficient D of the Kerr term and the maximum amplitude α of the mode. The corresponding results for waveguide channels with $t=0.1a_c$ can be obtained by replacing 0.087 on the far right hand side of Eqs. (52)–(54) by 0.187.

IV. WAVEGUIDE COUPLERS

A waveguide coupler is a circuit which transmits electromagnetic energy from one waveguide channel to another.[4] The circuit treated below is the photonic crystal circuit analogy of a coupling circuit which is of considerable interest in fiber-optics technology.

A schematic drawing of the coupler circuit is shown in Fig. 1(e). The two U-shaped waveguides couple to one another through weak interactions between sites along the parallel bottom parts of the U's. The separation between the bottom of the U's is a distance dr, and the sides of the two U's go off to infinity in opposite directions with no coupling interactions between them. The difference equations describing the waveguide coupler are: (i) For the sides of the U's

$$E_{jr,lr}=\gamma[\alpha(0,0)E_{jr,lr}+\alpha(0,r)(E_{jr,(l+1)r}+E_{jr,(l-1)r})], \tag{55}$$

where $j=0$ or N and $l=d+1,d+2,d+3,\ldots$ for d a positive integer giving the separations of the waveguide channels at their closest approach or $l=-1,-2,-3,\ldots$. (ii) For the bottom of the U's

$$E_{lr,jr}=\gamma[\alpha(0,0)E_{lr,jr}+\alpha(0,r)(E_{(l+1)r,jr}+E_{(l-1)r,jr}) + \delta E_{lr,j_0r}], \tag{56}$$

where $(j,j_0)=(d,0)$ or $(0,d)$ and $l=1,2,3,\ldots,N-2,N-1$. The boundary conditions joining the waveguide channels are

$$E_{0,dr}=\gamma[\alpha(0,0)E_{0,dr}+\alpha(0,r)(E_{r,dr}+E_{0,(d+1)r})+\delta E_{0,0}], \tag{57}$$

$$E_{0,0}=\gamma[\alpha(0,0)E_{0,0}+\alpha(0,r)(E_{r,0}+E_{0,-r})+\delta E_{0,dr}], \tag{58}$$

$$E_{Nr,dr}=\gamma[\alpha(0,0)E_{Nr,dr}+\alpha(0,r)(E_{Nr,(d+1)r}+E_{(N-1)r,dr}) + \delta E_{Nr,0}], \tag{59}$$

$$E_{Nr,0}=\gamma[\alpha(0,0)E_{Nr,0}+\alpha(0,r)(E_{Nr,-r}+E_{(N-1)r,0}) + \delta E_{Nr,dr}]. \tag{60}$$

The weak interaction between the two different waveguide channels is given by δ so that in the limit that $\delta=0$ the two channels have no interactions between them.

A solution of these equations is of the form

$$E_{0,lr}=ae^{ipl}+be^{-ipl}, \tag{61}$$

where $l=d+1,d+2,d+3,\ldots$;

$$E_{0,lr}=ce^{ipl}+d_ce^{-ipl}, \tag{62}$$

where $l=-1,-,2,-3,\ldots$;

$$E_{Nr,lr}=re^{ip|l|}, \tag{63}$$

where $l=d+1,d+2,d+3,\ldots$;

$$E_{Nr,lr}=ue^{ip|l|}, \tag{64}$$

where $l=-1,-2,-,3,\ldots$;

$$E_{lr,dr}=[i\sin(ql)x+\cos(ql)x_1]e^{ikl}+[-i\sin(ql)y + \cos(ql)y_1]e^{-ikl}, \tag{65}$$

where $l=0,1,2,\ldots,N$; and

$$E_{lr,0}=[\cos(ql)x+i\sin(ql)x_1]e^{ikl}+[\cos(ql)y - i\sin(ql)y_1]e^{-ikl}, \tag{66}$$

where $l=0,1,2,\ldots,N$. Here b and c are the amplitudes of the incident waves in the upper and lower waveguide channels, respectively, and r and u are the amplitudes of the waves transmitted in the upper and lower channels, respectively. The solutions in the region of the coupling, given in Eqs. (65) and (66), are generalizations to the discrete photonic crystal waveguide of the solution of the waveguide coupler problem in fiber-optics. A good discussion of the fiber-optic solution which is readily generalized to Eqs. (65) and (66) is in the text by Yeh.[4]

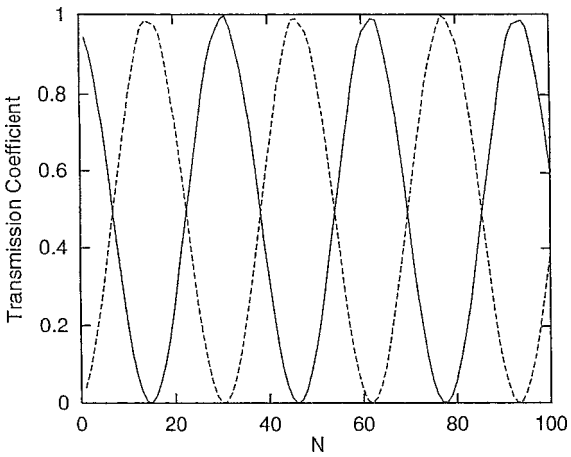

FIG. 6. Plot of $|r/b|^2$ (solid) and $|u/b|^2$ versus N for the waveguide coupler described in Eqs. (55)–(60).

Substituting Eqs. (61)–(66) into Eqs. (55)–(60) gives

$$\gamma=[\alpha(0,0)+2\alpha(r,0)\cos(p)]^{-1}, \tag{67}$$

$$\gamma=[\alpha(0,0)+2\alpha(r,0)\cos(q)\cos(k)]^{-1}, \tag{68}$$

$$2\alpha(r,0)\sin(q)\sin(k)=\delta. \tag{69}$$

Once the wave vector p is chosen, the dielectric (i.e., γ) is determined by Eq. (67). Then for fixed γ and δ, q and k are determined by Eqs. (67) and (68). For weak coupling (i.e., $\delta/\alpha(r,0)\ll 1$) $k\approx p$, and q is a small modulation causing a periodic transfer of the fields from one waveguide to the other and back. The wave forms given in Eqs. (67) and (68) are a linear combination of slowly varying $\sin q$ and $\cos q$ with coefficients x, x_1, y, y_1 determined by the difference equations and their boundary conditions.

Upon substituting Eqs. (61)–(66) into Eqs. (55)–(60) and eliminating x, x_1, y, and y_1 from the resulting set of linear equations, four equations are found which relate a, b, c, d_c, u, and r to one another. The reader is referred to the Appendix where these equations are listed as Eqs. (A1)–(A4). When the amplitudes b and c of the waves incident on the waveguide coupler are specified, the resulting set of four equations in four unknowns are solved for the reflected wave amplitudes a and c and the transmitted wave amplitudes r and u.

As an illustration of the theory, consider a coupler of length N, for which $b=1$ and $c=0$ in the small q, small δ limit. If $q=0.1$ so that $\cos q\approx 1$, then from Eqs. (67)–(69) $k\approx p$ with $\delta\approx 2q\alpha(r,0)\sin p$. The transmission coefficients for the two waveguide output channels are given from Eqs. (A1)–(A4) by $|r/b|^2$ and $|u/b|^2$ as functions of N for fixed k, p, q and coupler separation d which we take to be $d=5$. In Fig. 6 plots are presented for $|r/b|^2$ and $|u/b|^2$ versus N, using the Ref. 1 numerical data for the square lattice photonic crystal with $t=0.01a_c$ nearest-neighbor waveguide chan-

nels, for the case in which $p=k=\pi/4$ and $\omega a_c/2\pi c = 0.440$. The solid curve is for $|r/b|^2$ and the dashed curve is for $|u/b|^2$. As with fiber-optic waveguide couplers, the transmission is seen to oscillate between the two output waveguide lines as the length of the parallel coupler is increased.

The results in Fig. 6 exhibit an approximate periodicity. The wavelength in N is approximately 32 which corresponds to a wavenumber $2\pi/32=0.196\approx 2q$. Consequently, the wave first changes waveguide channels when the length of the coupler N equals $\pi/2q$. This is what is observed in the case of fiber-optics waveguides. (For an heuristic explanation of the physical process involved in these energy transfers the reader is referred to the text by Yeh.[4]) The terms in Eqs. (A1)–(A10) of the Appendix containing trigonometric functions with qN and $2qN$ arguments are associated with this periodicity. The effects of functions containing arguments of $kN\approx pN$ are less dominant in determining the periodicity properties of the transmission coefficient and reflection coefficients for the results shown in Fig. 6.

V. CONCLUSIONS

The localized electromagnetic modes in a number of different photonic crystal circuits have been studied using a recently developed difference equation method.[1] This is an alternative to approaches based on computer simulation methods[10–25] and allows for the treatment of particular types of large, complex photonic crystal circuits. Modes bound in waveguide channels formed from both linear and Kerr nonlinear media have been treated, and the theory resulting from these studies has been illustrated with numerical data from Ref. 1. A theory of waveguide couplers has been presented. In general the presentation in this paper completes the work presented in Ref. 1.

Two points to note are: (i). The photonic crystal circuits are actually generalizations of the optics of layer systems to more complex topologies. It is expected that a richer physical content will arise from this greater complexity. (ii) In the present formulation it is possible to design circuits which exhibit electromagnetic modes of a desired set of spatial field distributions and frequencies. This comes about because the natural way to solve the difference equations of our theory is to fix the frequency and fields distributions and solve for the dielectric contrasts needed to support the modal solutions that have these characteristics.

The results here are currently being developed to handle channels made of impurity materials of larger cross-sectional area in the plane perpendicular to the cylinder axes. This is a difficult problem, but its solution should result in a theory of great usefulness in the development of photonic crystal circuits. In this regard we note a recent review in which the future prospects of photonic crystal circuits is discussed.[13]

ACKNOWLEDGMENT

This work was funded in part by Department of Army Grant No. DAAD19-01-1-0527.

APPENDIX

The four equations obtained by substituting Eqs. (61)–(66) into Eqs. (55)–(60) and eliminating the coefficients x, x_1, y, and y_1 between the resulting set of equations are

$$[A_0(p)+A_1(N,p)]e^{ipd}a+[A_0(-p)+A_1(N,-p)]e^{-ipd}b+[B_0(p)-B_1(N,p)]c+[B_0(-p)-B_1(n,-p)]d_c+C(N,p)u+D(N,p)r=0, \tag{A1}$$

$$[B_0(-p)-B_1(N,-p)]e^{ipd}a+[B_0(p)-B_1(N,p)]e^{-ipd}b+[A_0(-p)+A_1(N,-p)]c+[A_0(p)+A_1(N,p)]d_c+D(N,p)e^{-ipd}u+C(N,p)e^{ipd}r=0, \tag{A2}$$

$$[A_0(p)+A_1(N+1,p)]e^{ipd}a+[A_0(-p)+A_1(N+1,p)]e^{-ipd}b+[B_0(-p)^*-B_1(N+1,p)^*]c+[B_0(p)^*-B_1(N+1,p)^*]d_c+C(N+1,p)e^{ip}u+D(N+1,p)e^{ip}r=0, \tag{A3}$$

and

$$[B_0(p)^*-B_1(N+1,p)^*]e^{ipd}a+[B_0(-p)^*-B_1(N+1,p)^*]e^{-ipd}b+[A_0(-p)+A_1(N+1,p)]c+[A_0(p)+A_1(N+1,p)]d_c+D(N+1,p)e^{-ipd}e^{ip}u+C(N+1,p)e^{ip(d+1)}r=0, \tag{A4}$$

where

$$A_0(p)=\frac{\sin(q)[\cos(q)-\cos(k)e^{ip}]}{2[\sin(q)^2-\sin(k)^2]}, \tag{A5}$$

$$A_1(N,p)=\frac{\sin(2Nq)}{4\sin[N(q-k))\sin(N(q+k)]}, \tag{A6}$$

$$B_0(p)=\frac{\sin(k)[\cos(q)e^{-ip}-\cos(k)]}{2[\sin(q)^2-\sin(k)^2]}-\frac{i}{2}, \tag{A7}$$

$$B_1(N,p)=\frac{[\sin(Nk)\cos(Nq)^2-i\cos(Nk)\sin(Nq)^2]e^{ikN}}{2\sin[N(q-k)]\sin[N(q+k)]}, \tag{A8}$$

$$C(N,p)=\frac{\sin(Nk)\cos(Nq)}{2\sin[N(q-k))\sin(N(q+k)]}, \tag{A9}$$

$$D(N,p)=-\frac{\sin(Nq)\cos(Nk)e^{ipd}}{2\sin[N(q-k)]\sin[N(q+k)]}. \tag{A10}$$

*FAX: 616-387-4939; email address: MCGURN@WMICH.EDU

[1] A.R. McGurn, Phys. Rev. B **61**, 13 235 (2000).
[2] A.R. McGurn, Phys. Lett. A **251**, 322 (1999).
[3] A.R. McGurn, Phys. Lett. A **260**, 314 (1999).
[4] Chai Yeh, *Applied Photonics* (Academic Press, San Diego, 1994), Chap. 11.
[5] H.G. Algul, M. Khazhinsky, A.R. McGurn, and J. Kapenga, J. Phys.: Condens. Matter **7**, 447 (1995).
[6] A.R. McGurn, Phys. Rev. B **53**, 7059 (1996).
[7] K.G. Khazhinsky and A.R. McGurn, Phys. Lett. A **237**, 175 (1998).
[8] S.F. Mingleev, Y.S. Kivshar, and R.A. Sammut, Phys. Rev. E **62**, 5777 (2000).
[9] A.J. Sievers and J.P. Page, *Dynamical Properties of Solids*, edited by G. Horton and A.A. Maradudin (Elsevier, Amsterdam, and New York, 1995), Vol. 7, p. 137.
[10] J.D. Joannopoulos, P.R. Villeneuve, and S. Fan, Nature (London) **386**, 143 (1997).
[11] *Photonic Gand Gaps and Localization*, edited by C.M. Soukoulis (Plenum, New York, 1992).
[12] *Photonic Band Gap Materials*, edited by C.M. Soukoulis (Kluwer and Academic, New York, 1995).
[13] G. Parker and M. Chalton, Phys. World **13**, 8 (2000).
[14] R.D. Meade, A. Devenyi, J.D. Joannopoulos, O.L. Alerhand, D.A. Smith, and K. Kash, J. Appl. Phys. **75**, 4753 (1994).
[15] S. Fan, J.N. Winn, A. Devenyi, J.C. Chen, R.D. Meade, and J.D. Joannopoulos, J. Opt. Soc. Am. B **12**, 1267 (1995).
[16] A. Mekis, J.C. Chen, I. Kurland, S. Fan, P.R. Villeneuve, and J.D. Joannopoulos, Phys. Rev. Lett. **77**, 3787 (1996).
[17] A. Mekis, S. Fan, and J.D. Joannopoulos, Phys. Rev. B **58**, 4809 (1998).
[18] S. Fan, P.R. Villeneuve, J.D. Joannopoulos, and H.A. Haus, Phys. Rev. Lett. **80**, 960 (1998).
[19] B.G. Levi, Phys. Today **52**, 21 (1999).
[20] S. Fan, S.G. Johnson, J.D. Joannopoulos, C. Manolatou, and H.A. Haus, J. Opt. Soc. Am. B **18**, 162 (2001).
[21] J. Yonekura, M. Ikeda, and T. Baba, J. Lightwave Technol. **17**, 1500 (1999).
[22] M.M. Segalas, R. Biswas, K.M. Ho, C.M. Soukoulis, D. Turner, B. Vasiku, S.C. Kothari, and S.Y. Lin, Microwave Opt. Technol. Lett. **23**, 56 (1999).
[23] A. Chutman and S. Noda, Appl. Phys. Lett. **75**, 3739 (1999).
[24] E. Chow, S.Y. Lin, S.G. Johnson, P.R. Villineneve, J.D. Joannopoulos, J.R. Wendt, G.A. Vawter, W. Zubrzycki, H. Haus, and A. Allenman, Nature (London) **407**, 983 (2000).
[25] A. Mekis, A. Dodabalapur, R.E. Slusher, and J.D. Joannopoulos, Opt. Lett. **25**, 942 (2000).